Lithos 260 (2016) 443–456

Contents lists available at ScienceDirect

Lithos

journal homepage: www.elsevier.com/locate/lithos

Zircon U–Pb geochronology, Sr–Nd–Hf isotopic composition and geological significance of the Late Triassic Baijiazhuang and Lvjing granitic plutons in West Qinling Orogen

Meng Duan [a,*], Yaoling Niu [a,b,c,**], Juanjuan Kong [b], Pu Sun [b], Yan Hu [b], Yu Zhang [d], Shuo Chen [b], Jiyong Li [b]

[a] School of Earth Sciences and Resources, China University of Geosciences, Beijing 100083, China
[b] Institute of Oceanology, Chinese Academy of Sciences, Qingdao, 266071, China
[c] Department of Earth Sciences, Durham University, Durham DH1 3LE, UK
[d] School of Earth Sciences, Lanzhou University, Lanzhou 730000, China

ARTICLE INFO

Article history:
Received 9 December 2015
Accepted 14 April 2016
Available online 7 May 2016

Keywords:
West Qinling Orogen
Late Triassic granitoid plutons
Lower crust melting
Slab break-off
Mantle wedge melting

ABSTRACT

The Qinling Orogen was a consequence of continental collision of the South China Craton with the North China Craton in the Triassic and caused widespread granitoid magmatism. However, the petrogenesis of these granitoids remains controversial. In this paper, we choose the Baijiazhuang (BJZ) and Lvjing (LJ) plutons in the West Qinling Orogen for a combined study of the zircon U–Pb geochronology, whole-rock major and trace element compositions and Sr–Nd–Hf isotopic characteristics. We obtained zircon crystallization ages of ~216 Ma and ~212 Ma for the BJZ and the LJ plutons, respectively. The granitoid samples from both plutons have high K_2O metaluminous to peraluminous compositions. They are enriched in large ion lithophile elements (LILEs), light rare earth elements (LREEs) and depleted in high field-strength elements (HFSEs) with significant negative Eu anomalies. The BJZ samples have initial Sr isotopic ratios of 0.7032 to 0.7078, $\varepsilon_{Nd}(t)$ of −10.99 to −8.54 and $\varepsilon_{Hf}(t)$ of −10.22 to −6.41. The LJ granitoids have initial Sr isotopic ratios of 0.7070 to 0.7080, $\varepsilon_{Nd}(t)$ of −5.37 to −4.58 and $\varepsilon_{Hf}(t)$ of −3.64 to −1.78. The enriched isotopic characteristics of the two plutons are consistent with their source being dominated by ancient continental crust. However, two BJZ samples show depleted Sr isotope compositions, which may infer possible involvement of mantle materials. Mantle-derived melt, which formed from partial melting of mantle wedge peridotite facilitated by dehydration of the subducted/subducting Mianlue ocean crust, provide the required heat for the crustal melting while also contributing to the compositions of these granitoids. That is, the two granitic plutons are magmatic responses to the closure of the Mianlue ocean basin and the continental collision between the Yangtze and South Qinling crustal terranes.

1. Introduction

The Qinling Orogen is the geological boundary between the North and the South China and is located in the middle of the Central Orogenic Belt on continental China (Jiang, 1994; Zhang and Liu, 1998). It was formed as a result of ultimate amalgamation of the Yangtze Block with the North China Craton through two separate collisional events along the Shangdan suture in the middle Paleozoic and the Mianlue suture in the Late Triassic (Fig. 1a, b; Dong et al., 2011; Ernst and Liou, 1995; Ernst et al., 2007; Faure et al., 2008; Jiang, 1994; Li et al., 2007; Mattauer et al., 1985; Meng and Zhang, 1999, 2000; Xiao et al., 2005, 2009; Zhang et al., 2004a, 2004b; Zhang and Liu, 1998;). There are widespread granitoids in the western segment of the Qinling Orogen or West Qinling Orogen (Fig. 1b), which record important information on the orogenesis (Dong et al., 2011, 2012a; Jiang et al., 2010; Meng and Zhang, 1999; Qin et al., 2009; Sun et al., 2002; Wang et al., 2013; Zhang et al., 2007). Crust–mantle interaction has been widely accepted as being responsible for the petrogenesis of these granitoids, i.e., they were derived from partial melting of the lower continental crust caused by heating from underplated mantle-derived melts (Cao et al., 2011; Jiang et al., 2010). However, controversies still exist on the origin of the mantle-derived melt (Dong et al., 2012a; Jiang et al., 2010; Li et al., 2007; Qin et al., 2008a, 2008b, 2009; Ratschbacher et al., 2003; Sun et al., 1998, 2002; Xue et al., 1996; Yang et al., 2014; Zhang et al., 2007; Zhu et al., 2011).

The decompression melting of the asthenosphere mantle, caused by the break-off of the Mianlue oceanic slab, has been a popular model invoked to infer the origin of mantle-derived melt (Dong et al., 2011; Sun et al., 2002; Zhang et al., 2007, 2009). The slab break-off as a trigger is possible, but whether this can induce significant asthenospheric passive upwelling and decompression melting is not as straightforward as generally perceived without question.

In this paper, we provide high quality zircon in situ U–Pb age data, whole-rock major and trace element data and Sr–Nd–Hf isotope compositions of representative granitoid samples from the Baijiazhuang (BJZ) and the Lvjing (LJ) plutons in the West Qinling Orogen to discuss

* Corresponding to: M. Duan, School of Earth Sciences and Resources, China University of Geosciences, Beijing, 100083, China.
** Correspondence to: Y. Niu, School of Earth Sciences and Resources, China University of Geosciences, Beijing, 100083, China.
E-mail addresses: m.duan@foxmail.com (M. Duan), yaoling.niu@foxmail.com (Y. Niu).

http://dx.doi.org/10.1016/j.lithos.2016.04.015
0024-4937/

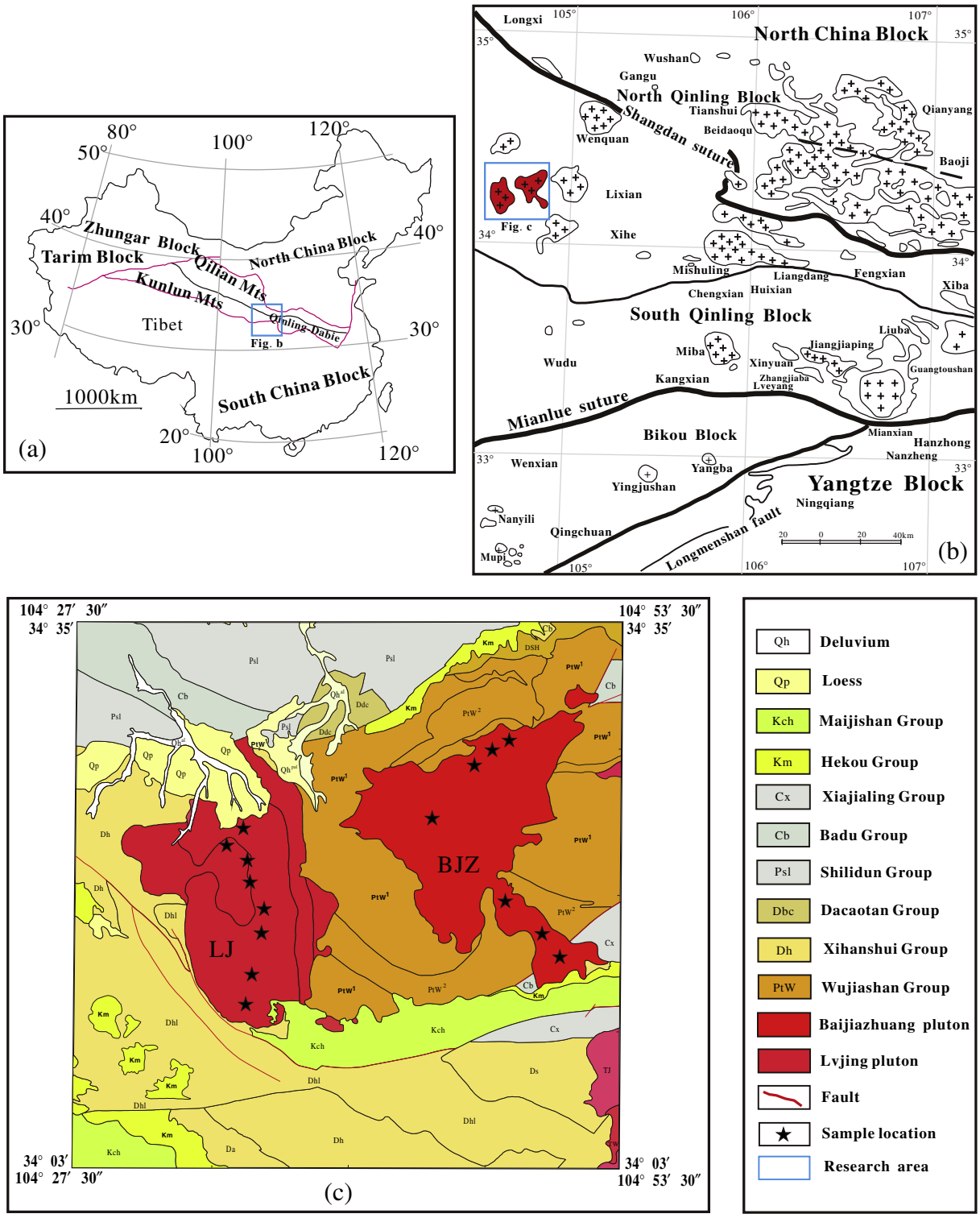

Fig. 1. (a) Simplified geological framework of continental China (after Qin et al., 2009). (b) Simplified geological map showing the distribution of Triassic granitoids in the West Qinling Orogen (after Qin et al., 2009). (c) Geological map of the Baijiazhuang (BJZ) and Lvjing (LJ) plutons (after 1:250,000 geological map of Mianxian, Chinese Geological Survey, 2007).

the petrogenesis of these granitoids. We propose that mantle wedge melting facilitated by addition of water from the subducted Mianlue seafloor resulted in the mantle-derived melt with basaltic compositions, whose ascent and underplating caused the lower continental crust melting for the widespread granitoid magmatism. This interpretation may be simplistic but can effectively explain the observations while also alleviating the physical difficulties associated with the popular slab break-off model.

2. Geological background and petrology of the granitoids

2.1. Geological background

The Qinling Orogen links the Dabie–Sulu Orogen in the east and the Kunlun–Qilian Orogen in the west (Fig. 1a) and has been divided into the North and South Qinling Blocks by the Shangdan suture zone (Fig. 1b; Dong et al., 2011, 2013; Meng and Zhang, 1999, 2000; Qin

et al., 2008a; Zhang et al., 2007). The South Qinling block collided with the North Qinling block in the Middle Paleozoic along the Shangdan suture (Fig. 1b). The South Qinling block was separated from the South China block during the Carboniferous to early Triassic by the paleo-Tethyan Qinling ocean (Meng and Zhang, 1999). After the closure of the paleo-Tethyan Qinling ocean, the South China block collided with the South Qinling block in the Late Triassic along the Mianlue suture, which resulted in the widespread granitic magmatism and the final amalgamation China continent (Meng and Zhang, 1999). A series of ophiolites fragments occur in the Mianlue suture zone, which have been explained to represent the remnants of the paleo-Tethyan Qinling ocean (Lai et al., 2008; Xu et al., 2002). The South Qinling block consists of Late Paleozoic medium-grade metasedimentary and metavolcanic rocks and the Triassic granitoids (Li and Sun, 1996; Mattauer et al., 1985; Qin et al., 2009). The BJZ and the LJ are two plutons of these granitoids crop out in an area of ~200 km^3 in the West Qinling Orogen. The BJZ pluton intruded the Wujiashan Group (Fig. 1c), which is a Mesoproterozoic strata in the research area and mainly consists of banded marble, thick layered quartz marble and mica quartz schist. The LJ pluton intruded the Devonian Xihanshui Group, which consists of thick layers of limestone, calcareous sandstone, siltstone, silty shale, limestone and marlstone (Xu et al., 2006).

2.2. Petrology of the granitoids

The BJZ and the LJ plutons mainly consist of medium-coarse grained biotite granite. The BJZ pluton comprises quartz (~25%), plagioclase (~30%), K-feldspar (~35%) and minor amphibole and biotite (~5%) with accessory apatite, zircon, sphene and magnetite. Compared with the BJZ pluton, the LJ pluton has similar mineral assemblages and modes except for lower modes of quartz (~20%) and higher modes of plagioclase (~35%) (Fig. 2a, b, c, and d). The LJ pluton also contains fine-grained mafic magmatic enclaves (MMEs) (Fig. 2e, f). These MMEs are 5–20 cm in size and have the same mineralogy but more mafic mineral modes (more amphibole and biotite) and higher amount of Ti-Fe oxide and apatite than the granitoid host.

3. Analytical methods

The freshest granitoid samples were chosen for geochemical analysis. Weathered surfaces, pen marks and saw marks were ground off and thoroughly cleaned. The samples were then crushed to ~1 cm^3 size fragments and repeatedly washed with Milli-Q water in an ultrasonic bath before being dried and ground into powders with an agate mill in a clean environment.

3.1. Major and trace element analysis

Major and trace element analysis was done at China University of Geosciences in Beijing (CUGB). Whole-rock major elements were analyzed using a Leeman Prodigy Inductively Coupled Plasma Optical Emission Spectroscopy (ICP-OES) with the elemental analysis accuracy better than 5%. Analysis of USGS reference rock standards BCR-1, AGV-2 and national geological standard reference materials GSR-3 give precisions (1σ) better than 1% for most elements except for TiO_2 (~1.5%) and P_2O_5 (~2%).

Trace elements were analyzed using an Agilent-7500a ICP–MS. BCR-1 and BHVO-1 were used to monitor the analytical accuracy and precision. Analytical accuracy, as indicated by relative error between measured and recommended values, is better than 5% for most elements, ranging between 10% and 13% for Cu, Sc, Nb, Er, Th, and U and between 10% and 15% for Ta, Tm, and Gd (see Song et al., 2010b).

3.2. Sr–Nd–Hf isotopic analysis

The bulk-rock Sr–Nd–Hf isotopic compositions were analyzed at the Guangzhou Institute of Geochemistry, Chinese Academy of Sciences (GIG-CAS).

The Sr and the rare earth elements (REE) were separated with cation columns, and HDEHP-coated Kef columns were used for further Nd separation. The purified Sr and Nd were diluted in 2% HNO_3 for analysis with a Neptune ICP–MS by using a Meinhard glass nebulizer with an uptake rate of 0.1 mL/min. The Hf was separated from other elements using combination of Eichrom RE and HDEHP columns. The Hf isotopic compositions were analyzed using a Neptune MC–ICP–MS following the analytical procedure of Li et al. (2009). The measured Sr–Nd–Hf isotopic ratios were normalized to $^{86}Sr/^{88}Sr = 0.1194$, $^{146}Nd/^{144}Nd = 0.7219$ and $^{179}Hf/^{177}Hf = 0.7325$, respectively. See Li et al. (2006) for details of analytical procedures.

3.3. Zircon LA–ICP–MS U–Pb dating

Two granitoid samples from the Baijiazhuang (BJZ12-04) and Lvjing (DHG12-01) plutons were chosen for zircon U–Pb dating at CUGB. The instrument couples a quadrupole ICP–MS (Agilient 7500a) and an UP-193 Solid-State laser (193 nm, New Wave Research Inc.) with an automated positioning system (Song et al., 2010a). During the analysis, laser spot size was set at ~36 μm with laser energy density at 8.5 J/cm^2 and repetition rate at 10 Hz. The specific procedure of laser sampling is 5-s pre-ablation, 20-s flushing sample-chamber and 40-s data collection. The high-purity helium gas stream was used with flux of 0.8 L/min, and the ablated material was carried into the ICP–MS. In order to ensure energy stability, the whole laser path was fluxed with N_2 (15 L/min) and Ar (1.15 L/min). The counting time for U, Th, ^{204}Pb, ^{206}Pb, ^{207}Pb and ^{208}Pb is 20 ms, and is 15 ms for other elements (Song et al., 2010a). Zircon 91500 is used as external standard to correct for U–Pb isotope fractionation effects (Wiedenbeck et al., 1995). The isotopic ratios and element concentrations of zircon were calculated with GLITTER 4.4. The concordia ages and diagrams were made using Isoplot/Ex (3.0) (Ludwig, 2003).

4. Results

4.1. Zircon LA–ICP–MS U–Pb ages

Representative CL images of analyzed zircons are shown in Appendix 1, and the U–Pb ages are given in Appendix 2.

Zircons from sample BJZ12-04 (from the BJZ pluton) are subhedral to euhedral. They have varying sizes of 100 to 300 μm, length/width ratios of 2:1 to 6:1 and clear oscillatory zoning in the CL images (Appendix 1), suggesting a magmatic origin (Corfu et al., 2003; Pupin, 1980). Twenty-five zircons show varying U (374–3728 ppm), Th (93–1436 ppm) and Th/U (0.1–1.1; mostly less than 1). Nineteen analyses of 25 zircons give a weighted average $^{206}Pb/^{238}U$ age of 216 ± 1.8 Ma (2σ; MSWD = 1.5), which is interpreted as the crystallization age of the BJZ pluton (Fig. 3). The other six analyses with discordance > 10% (Appendix 2) were rejected to plot into the Concordance diagram.

Zircons from sample DHG12-01 (from the LJ pluton) are more euhedral than those from the BJZ pluton. They are ~100 to 300 μm in size and have varying length/width ratio of 1:1–3:1 (Appendix 1). They show clear oscillatory zoning in the CL images, which is also indicative of a magmatic origin (Corfu et al., 2003). Thirty zircons show varying U (143–1412 ppm), Th (81–433 ppm) and Th/U (0.25–0.96). The ages of LJ samples plot in two groups with ages of ~225 Ma and ~212 Ma, respectively, with an average age of 217.5 ± 2.5 Ma (Fig. 3b). The bimodal ages may represent two batches of magmatic events (e.g., a composite pluton). We interpret the ~212 Ma as representing the final crystallization age of the LJ pluton, and zircons of ~225 Ma may represent "xenocrysts" from prior batch of magma.

4.2. Major and trace elements

Appendix 3 gives the analytical data.

The samples from the BJZ pluton have high SiO_2 (72.58–76.60 wt.%), Al_2O_3 (12.07–14.91 wt.%), total alkalis ($Na_2O + K_2O$ = 8.29–9.01 wt.%)

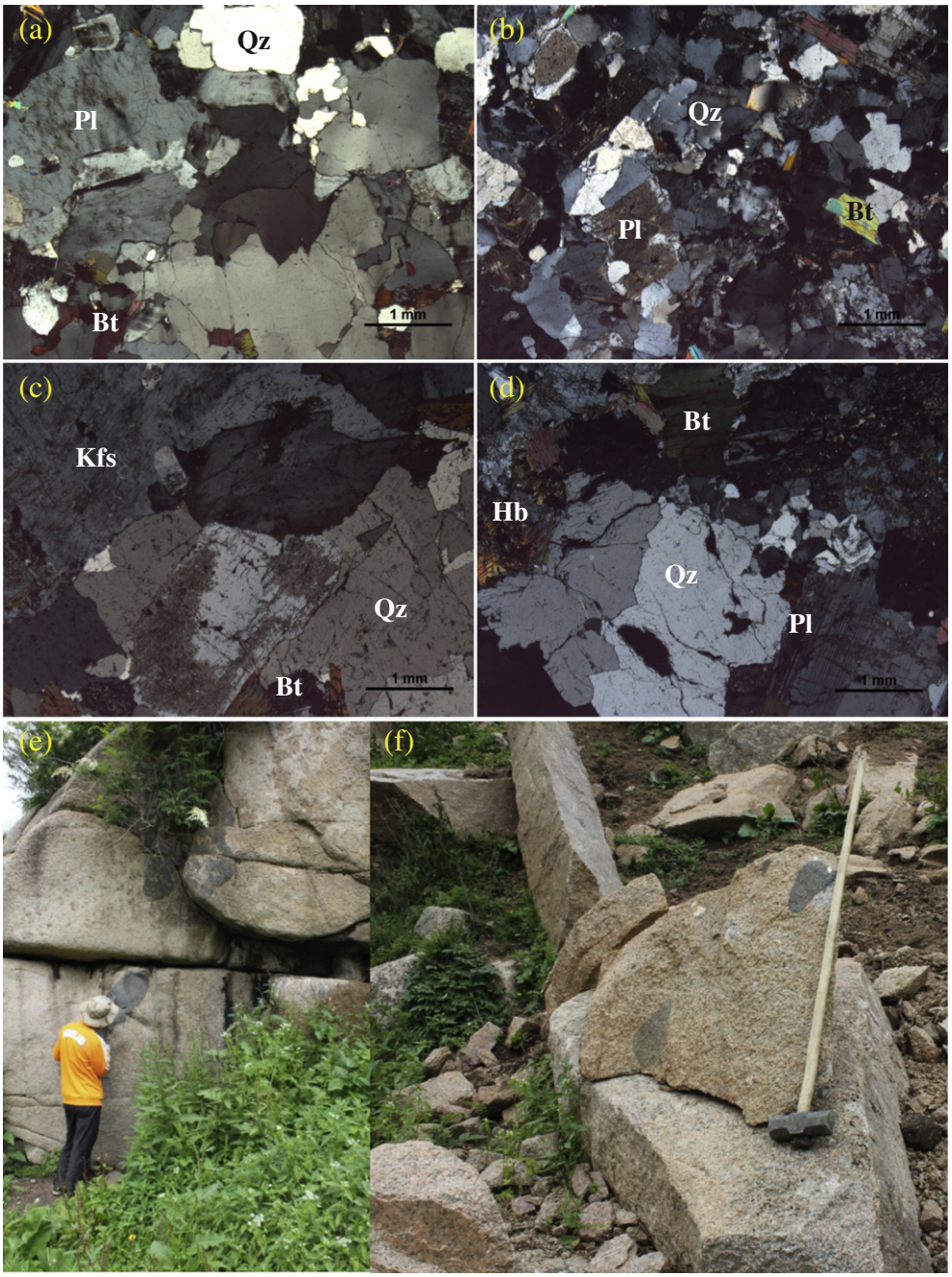

Fig. 2. Photomicrographs of granitoid samples from the BJZ (a, b) and LJ (c, d) plutons. Field photos of MMEs in the host of the LJ pluton (e, f).

and K_2O/Na_2O (1.30–1.72) and low TiO_2 (0.12–0.18 wt.%), MgO (0.16–0.33 wt.%), Fe_2O_{3T} (0.88–1.31 wt.%) and CaO (0.62–0.98 wt.%) (Appendix 3). They plot in the granite field in the TAS diagram (Fig. 4a). The aluminum saturation index (ASI = molar Al_2O_3 / (Na_2O + K_2O + CaO)) varies from weakly metaluminous to peraluminous (Fig. 4b).

Samples from the LJ pluton, on the other hand, have relatively lower SiO_2 (69.52–71.95 wt.%), total alkalis (7.56–8.74 wt.%), K_2O/Na_2O (1.36–1.55) and relatively higher TiO_2 (0.25–0.37 wt.%), MgO (0.64–0.91 wt.%), Fe_2O_{3T} (1.96–2.82 wt.%) and CaO (1.43–1.99 wt.%) (Fig. 5). They plot in the granite (Fig. 4a) and peraluminous fields (Fig. 4b) with ASI > 1 (0.99–1.12). Compared with the granitoid host, the MMEs from the LJ pluton have lower SiO_2, total alkalis and higher TiO_2, Al_2O_3, CaO, MgO and Fe_2O_{3T}, with a small $Mg^{\#}$ (=molar $100*Mg^{2+}$ / [Fe^{2+} + Mg^{2+}]) variation (52.7–53.4) (Appendix 3; Fig. 5). They plot in the monzonite and granodiorite fields (Fig. 4a) and in the metaluminous field (Fig. 4b).

In chondrite-normalized REE diagrams (Fig. 6a, c), granitoid samples from the BJZ and the LJ plutons show LREE enrichment and HREE depletion with large $(La/Yb)_N$ variations of 11.19–30.75 and 13.24–22.87, respectively. All the samples show flat HREE patterns with $(Dy/Yb)_N$ ~ 1.09–1.65 for the BJZ pluton and ~1.29–1.51 for the LJ pluton, suggesting the absence of garnet in their petrogenesis. Negative Eu anomalies exist in all the granitoid samples. However, samples from the BJZ pluton have greater negative Eu anomalies (Eu/Eu^* = 0.23–0.43; $Eu/Eu^* = 2Eu_N / (Sm_N + Gd_N)$) than those from the LJ pluton (Eu/Eu^* = 0.47–0.78). The MMEs show similar REE patterns with DHG12-06 and DHG12-09 showing moderate and weak negative Eu anomalies, respectively.

In the primitive mantle normalized multi-element diagrams (Fig. 6b, d), samples from both plutons show spikes of large ion lithophile elements (LILE; e.g., Th, U, K, Pb) and toughs of high field-strength elements (HFSE; e.g., Nb, Ta, Ti, P), resembling the bulk continental crust (BCC; Rudnick and Gao, 2003). The two MMEs from the LJ pluton show

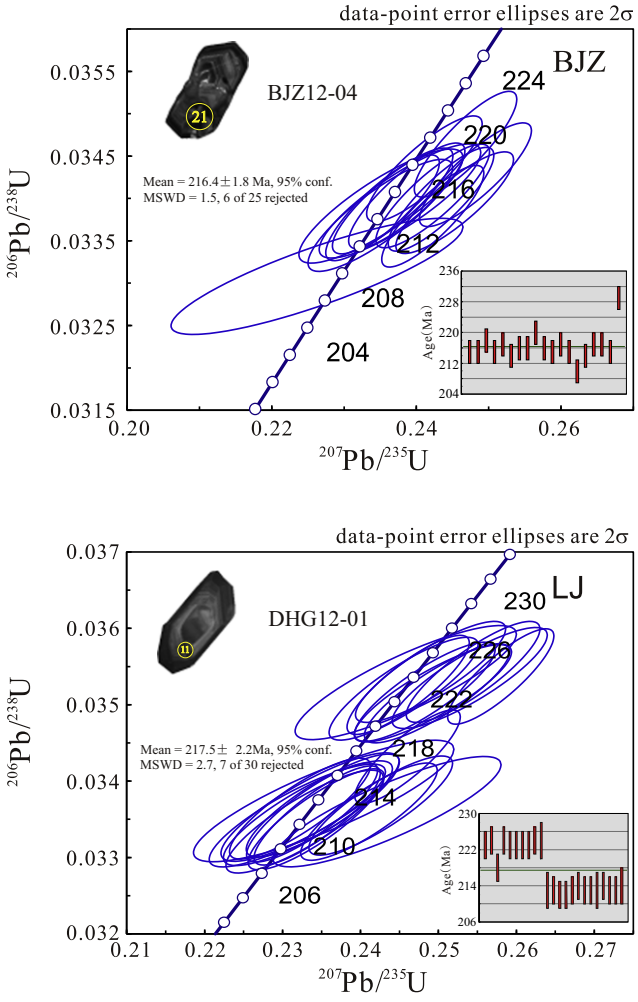

Fig. 3. LA–ICP–MS U–Pb concordia diagrams for zircons from the BJZ and the LJ plutons.

similar trace element patterns with the host granites but with weak or absence of toughs of P and Ti, which is consistent with the higher modes of apatite and Fe-Ti oxides in the MMEs.

4.3. Bulk-rock Sr–Nd–Hf isotopes

Isotopic compositions of all the analyzed samples are given in Appendix 4 and shown in Fig. 7a, b.

The samples from the BJZ pluton have initial Sr isotopic ratios of 0.7033–0.7068, $\varepsilon_{Nd}(t)$ of −10.95 to −8.50 and $\varepsilon_{Hf}(t)$ of −10.14 to −6.33. Whole-rock Nd isotope model ages (T_{DM}) range from 1.6 to 2.2 Ga. Single stage Hf model ages (T_{DM1}) are from 1.3 to 1.7 Ga and two stage Hf model ages (T_{DM2}) are from 1.7 to 1.9 Ga.

The granitoids from the LJ pluton have relatively uniform Sr ($(^{87}Sr/^{86}Sr)_i$ ~ 0.7070–0.7079), Nd ($\varepsilon_{Nd}(t)$ ~ −5.35 to −4.56) and Hf ($\varepsilon_{Hf}(t)$ ~ −3.59 to −1.74) isotopes. The whole-rock Nd isotopic model ages (T_{DM}) are essentially the same of ~1.3–1.4 Ga, so are the single stage Hf model ages (T_{DM1} ~ 1.0–1.1 Ga) and two stage Hf model ages (T_{DM2} ~ 1.5–1.6 Ga).

The two MMEs from the LJ pluton have similar Nd ($\varepsilon_{Nd}(t)$ ~ −4.90 to −3.52) and Hf ($\varepsilon_{Hf}(t)$ ~ −1.34 to +2.41) isotopes, but rather different Sr isotopic compositions with DHG12-06 being much more radiogenic ($(^{87}Sr/^{86}Sr)_i$ of 0.7161 (Fig. 7a), which may result from addition of upper crust materials during magma evolution or during the production of mantle-derived melt (see below).

5. Discussion

5.1. Origin of the LJ MMEs

The origin of the MMEs in granitoids has long been debated. One popular explanation is magma mixing between mafic and felsic magmas (Baxter and Feely, 2002; Dong et al., 2011; Qin et al., 2008a, 2009; Vernon, 1984; Zhang et al., 2007). However, this mechanism cannot explain the widely observed rather similar/overlapping isotopic compositions between the MMEs and the granitoid host simply because it is physically unlikely that isotopic are homogenized while major and trace elements are not during magma mixing (Niu et al., 2013). Another interpretation is that MMEs represent cumulates from more primitive andesitic melt of the same magmatic system (Barbarin, 2005; Chen et al., 2015; Huang et al., 2014; Niu et al., 2013).

The MMEs in the LJ pluton have no chilled margins at contacts with the host granitoids. They are elliptical and have similar mineral assemblages as the granitoids but with greater mafic (e.g., amphibole) mineral modes, indicating that the MMEs in the LJ pluton were not formed by magma mixing (Chen et al., 2015; Niu et al., 2013). Because of the first order correlated variations in major elements of MMEs and host granitoids (Fig. 5), and similar REE and trace element patterns (Fig. 6), we consider the MMEs are consistent with being of cumulate origin from an earlier batch of andesitic melt (also see Chen et al., 2015).

The high $(^{87}Sr/^{86}Sr)_i$ of MME DHG12-06 likely represents cumulate from a parental magma with high $(^{87}Sr/^{86}Sr)_i$, which may result from greater extent of crustal assimilation although we cannot rule out the possibility of terrigenous sediment contribution to mantle wedge

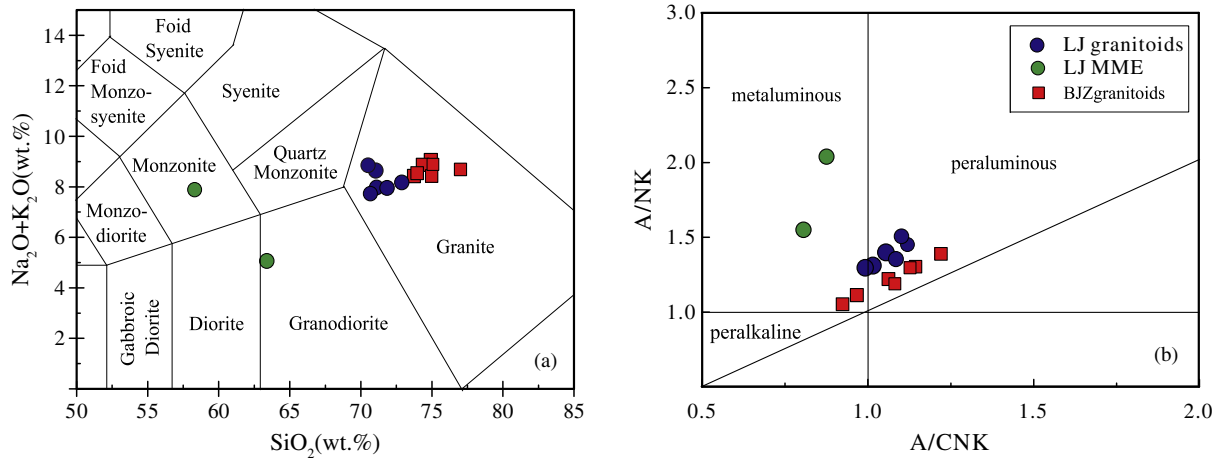

Fig. 4. (a) TAS diagram and (b) A/NK [molar ratio $Al_2O_3/(Na_2O + K_2O)$] vs. A/CNK [molar ratio $Al_2O_3/(CaO + Na_2O + K_2O)$] of granitoids from the BJZ and the LJ plutons.

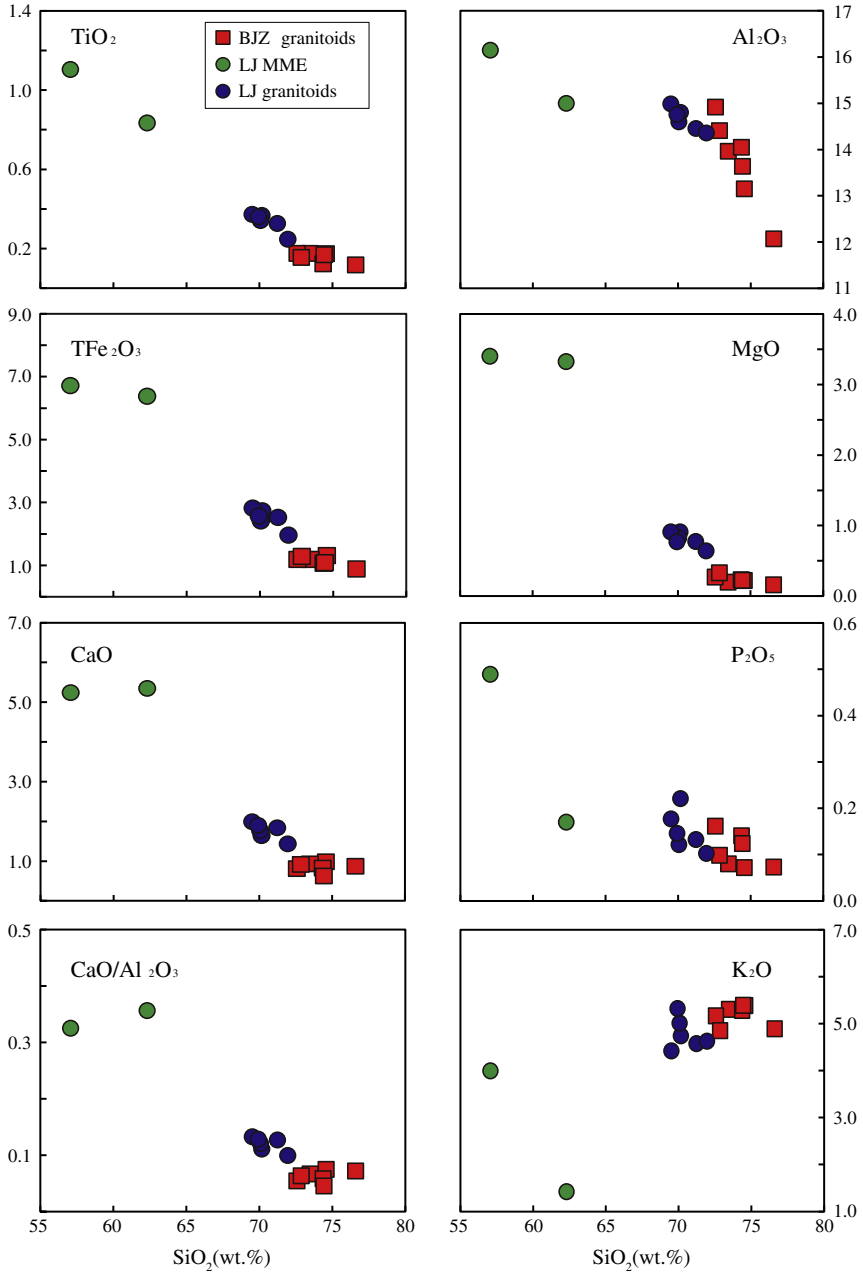

Fig. 5. SiO_2 variation diagrams of major element oxides of the BJZ and the LJ plutons.

melting source region for mantle-derived melt (see below). If the parental magmas represent early batches of melt intruding the crustal magma chamber, it would have been assimilated more of the crust materials with evolved Sr isotopic compositions inherited in the cumulated MMEs. These MMEs can be captured by the granitic melt later intruded in the magma chamber and then fractionated from the granitic melt together with the minerals crystallized. Generally, MME DHG12-06 and the granites are accumulated from different batches of magmas with different isotopic compositions in a periodically replenished magma chamber.

5.2. Petrogenesis of the BJZ and the LJ plutons

5.2.1. Crystallization evolution

As mentioned above, the granitoids from the BJZ pluton are relatively more felsic than those from the LJ pluton (Fig. 5), which are consistent with their crystallizing from a more evolved parental magma than the LJ samples. Compared with the samples from the LJ pluton, those from the BJZ pluton exhibit lower Sr content and more significant negative Sr anomalies with Sr/Sr^* ($=2Sr_N / [Pr_N + Nd_N]$) 0.18–0.35 (Figs. 6 and 8), corresponding to greater negative Eu anomalies (Fig. 8), which is consistent with the BJZ samples being more evolved with a greater extent of plagioclase fractionation. One MME (DHG12-06) shows higher Sr/Sr^* and Eu/Eu^* than the granitoid host, and the other MME (DHG12-09) has intermediate Sr/Sr^* and higher Eu/Eu^* (Fig. 8), which are consistent with their cumulating origin in the early stage of the magma evolution (see above).

5.2.2. Source of the granitoids

The granite samples are enriched in LILEs (Th, U, K, Pb) and LREEs and depleted in HFSEs (Nb, Ta, Ti, P) (Fig. 6), similar to the continental crust. In the $(^{87}Sr/^{86}Sr)_i$ vs. $\varepsilon_{Nd}(t)$ diagram (Fig. 7a), isotopic compositions of other Triassic granitic plutons in the Qinling Orogen are plotted for comparison (e.g., the Guangtoushan-Liuba, Mishuling and Wenquan plutons; Cao

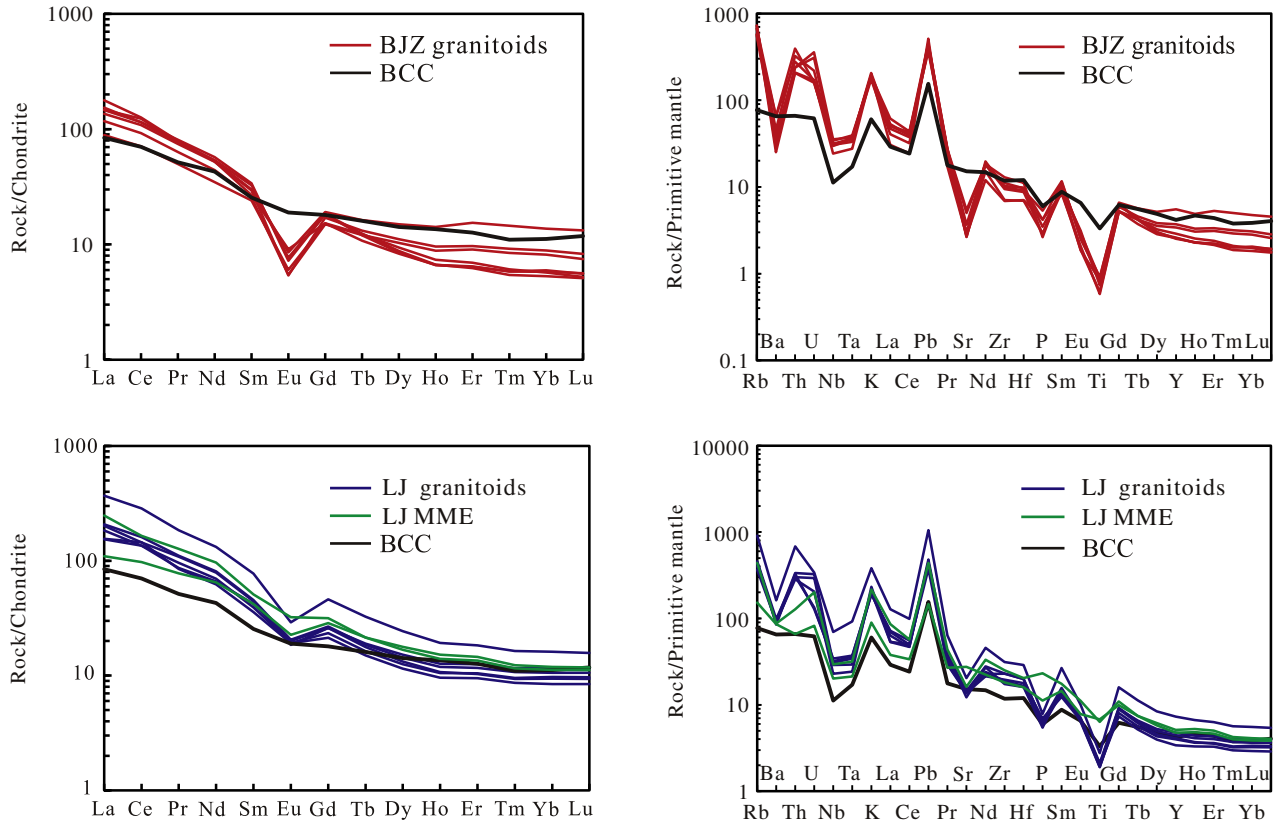

Fig. 6. Chondrite-normalized REE patterns (a, c) and primitive-mantle normalized trace element patterns (b, d) for granitoids of the BJZ and the LJ plutons. Bulk continental crust (BCC) is from Rudnick and Gao (2003); chondrite and primitive mantle values are from Sun and McDonough (1989).

et al., 2011; Qin et al., 2009; Zhang et al., 2006). The granitoid samples of the BJZ and the LJ plutons, similar to other granitoids in the Qinling Orogen, have evolved isotopic compositions with $(^{87}Sr/^{86}Sr)_i$ of most samples ranging from 0.704 to 0.710, negative $\varepsilon_{Nd}(t)$ (−10.95 to −8.50) and $\varepsilon_{Hf}(t)$ (−10.14 to −6.33) (Fig. 7), which is consistent with these granitoids being derived from lower continental crust (Qin et al., 2009; Wang et al., 2013; Zhang et al., 2007). The whole-rock Nd isotopic model ages (T_{DM}; 1.6–2.2 Ga and 1.3–1.4 Ga, respectively) and single stage Hf model ages (T_{DM1}; 1.3–1.7 Ga and 1.0–1.1 Ga, respectively) of BJZ and LJ granites also support a source composed of ancient lower continental crust (Qin et al., 2009; Zhang et al., 2007). The two stage Hf model ages (T_{DM2}) of BJZ and LJ granites are 1.7–1.9 Ga and 1.5–1.6 Ga, respectively, suggesting the granites deriving from reworking of Late Palaeoproterozoic to Early Mesoproterozoic crust. However, several samples that have lower $(^{87}Sr/^{86}Sr)_i$ (e.g., BJZ12-04, LZG12-07) or higher $\varepsilon_{Nd}(t)$ (> −10) (Fig. 7a) indicate that the lower continental crust is not their only source component and materials with depleted isotopic compositions must have been involved in the melting process. Such depleted materials are most probably mantle derived (Qin et al., 2008b; Sun et al., 2002).

5.2.3. Origin of mantle-derived melt

Granitoid magmatism in the continental collision belts is explained to result from lithospheric delamination (Bird, 1979) or break-off

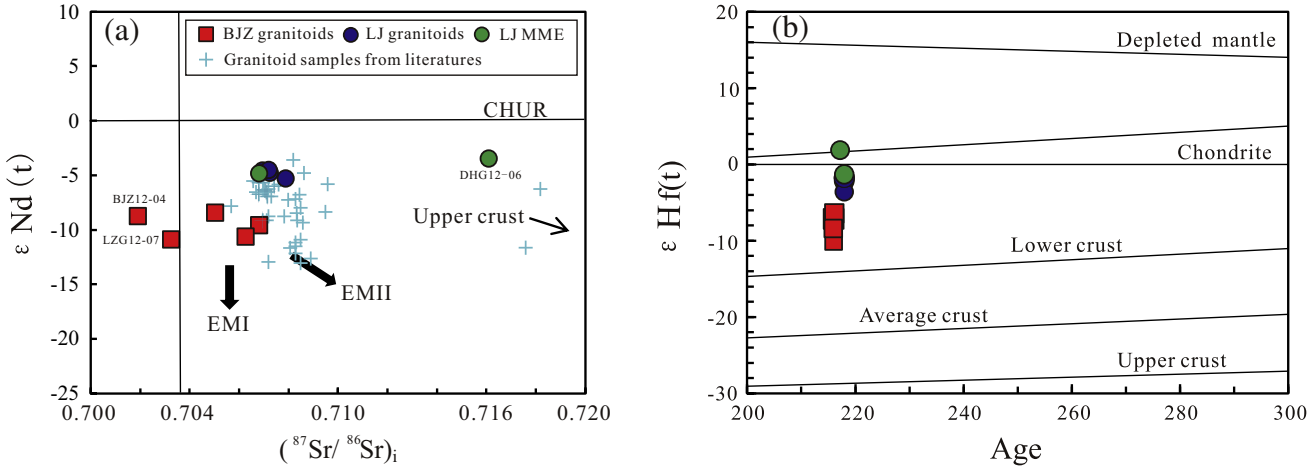

Fig. 7. (a) Initial $(^{87}Sr/^{86}Sr)$ vs. $\varepsilon_{Nd}(t)$ of granitoids of the BJZ and the LJ plutons. For comparisons isotope compositions of the Guangtousshan–Miba pluton (Zhang et al., 2006), the Mishuling pluton (Qin et al., 2009) and the Wenquan pluton (Cao et al., 2011) in the West Qinling Orogen are also plotted. (b) Age vs. $\varepsilon_{Hf}(t)$ of the BJZ and the LJ plutons.

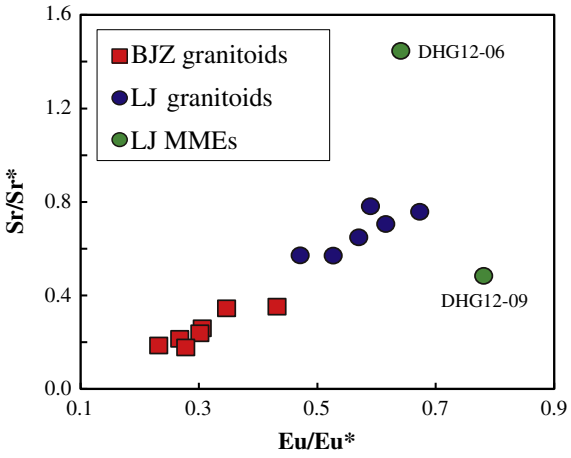

Fig. 8. Eu/Eu* vs. Sr/Sr* of granitoids from the BJZ and the LJ plutons, $Eu/Eu^* = 2Eu_N/(Sm_N + Gd_N)$, $Sr/Sr^* = 2Sr_N/(Pr_N + Nd_N)$ following Niu and O'Hara (2009).

of the oceanic slab from the buoyant continental lithosphere (Davies and von Blanckenburg, 1995). In Bird (1979), the delamination of continental lithospheric mantle is invoked to provide a conduit enabling the asthenosphere to arise to the base of the continental crust and induce granitoid magmatism. However, the delamination of the continental lithospheric mantle is physically difficult because the lithospheric mantle with high $Mg^{\#}$ and low Al_2O_3 content has lower density relative to the underlying asthenosphere due to the history of high extent melt extraction (Niu and O'Hara, 2008; Niu et al., 2003).

Asthenosphere upwelling induced by the oceanic slab break-off is more widely used in interpreting the granitoid magmatism in the continental collision belt (Davies and von Blanckenburg, 1995; Dong et al., 2011; Sun et al., 2002; Zhang et al., 2007, 2009). However, this model also has problems. First, slab break-off cannot produce stationary lithospheric window adequate for continued asthenospheric upwelling and decompression melting as it would take place beneath ocean ridges (Klein and Langmuir, 1987; McKenzie and Bickle, 1988; Niu and Batiza, 1991; Niu and O'Hara, 2008). Therefore, the amount of mantle-derived melt produced by slab break-off must be limited in volume and cannot be an effective cause for significant crustal melting required by the widespread and voluminous granitoid magmatism in the West Qinling orogenic belt (Zhang et al., 2007; Fig. 1b). Furthermore, the absence of high pressure metamorphic rocks in the Qinling orogen indicates that the slab break-off, if there was any, happened at a shallow depth, which has been explained to enable the upwelling asthenosphere to impinge on the base of lower continental crust (Qin et al., 2008a, 2008b; Sun et al., 2002). However, as we mentioned above, asthenosphere cannot simply heat the crust to melt without removing the buoyant continental lithospheric mantle.

Here we propose a much simpler model that is consistent with the observations and basic petrological concepts. That is, ascent and underplating of basaltic melt of mantle wedge origin can cause lower continental crust melting to account for the granitoids. When the Mianlue oceanic slab subducted beneath the South Qinling Block, dehydration of the ocean crust can effectively lower the solidus of mantle wedge peridotite to melt for the basaltic melt (e.g., Pearce and Peate, 1995). Extraction, ascent and underplating of such mantle wedge-derived basaltic melt can induce the lower continental crustal melting to produce magmas parental to the BJZ and the LJ granitoids (Fig. 9). Such mantle-derived melt, also contributes materials to the granitoid magmatism, i.e., there exists mixing between the mantle-derived isotopically depleted melt and isotopically enriched felsic melt from the lower continental crust, which is consistent with variable isotope compositions (Fig. 7).

Furthermore, terrigenous sediment, which may transports as melt or fluid from the subducted ocean slab to the overlying mantle wedge (Elliott, 2003; Johnson and Plank, 2000; Lee and Anderson, 2015; Niu et al., 2013; Nichols et al., 1994) and give the mantle-derived melt isotopically more enriched character, has long been recognized to contribute to the source of the island arc basalts (IAB) (Davidson, 1996; Elliott, 2003; Morris et al., 1990; Vroon et al., 1993). Such mantle-derived melt, when mixing with a high proportion with the melt from the lower continental crust, can crystalize mineral assemblages with enriched isotopic characters (e.g., MME DHG12-06; Fig. 7a).

5.2.4. Implications for the division of syn-collisional or post-collisional granitoids

Many studies refer the formation stage of the granitic plutons as syn-collisional or post-collisional using various geochemical discrimination diagrams (Barbarin, 1999; Dong et al., 2011, 2012a; Harris et al., 1986; Maniar and Piccoli, 1989; Pearce et al., 1984; Qin et al., 2008a; Zhang et al., 2007; Zhu et al., 2011). However, collision by itself does not generate sufficient heat, creates no scenario for decompression nor source of water addition and, thus, cannot produce large volumes of granitic magmas (Niu, 2005). The precise timing to distinguish syn-collisional and post-collisional processes is in itself vague and cannot be constrained. The ages of Triassic granites in the Qinling Orogen have been popularly invoked as representing the time of oceanic slab

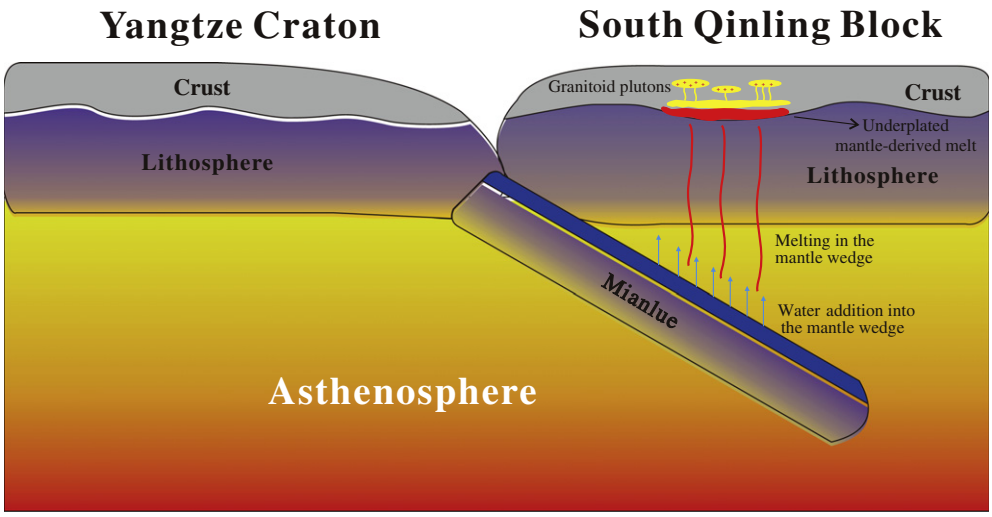

Fig. 9. Simple tectonic cartoon shows the formation of mantle-derived melt, partial melting of the lower continental crust and formation of widespread granitoids in the West Qinling Orogen.

break-off after the collision, with the assumption that slab break-off induced the upwelling of asthenospheric mantle and thus the formation of widespread Triassic granitic plutons in the Qinling Orogen (Qin et al., 2008b; Sun et al., 2002). However, such an assumption on the petrogenesis of Triassic granites in the Qinling Orogen is far from robust as discussed above. Thus, even though there may be some genetic relationship between the collision and the granitoid magmatism, caution is needed when applying the geochemical or chronological data to "constrain" the nature and timing of the events that actually cannot yet be constrained, for which genuine efforts are needed in future studies.

6. Conclusion

(1) Zircon U–Pb dating give ages of ~216 and 212 Ma for the BJZ and the LJ plutons, respectively.
(2) The MMEs in the LJ pluton represent cumulate from the more primitive andesitic melt in the early stage of the magmatic evolution.
(3) The enriched Sr–Nd–Hf isotope compositions suggest that their main source is the ancient lower continental crust. However, components from depleted mantle wedge and upper crust materials must have been involved in the formation process of the granitic magmas.
(4) We emphasize that seafloor slab dehydration induced mantle wedge melting remains the primary mechanism for mantle-derived basaltic melts, whose underplating and intrusion of the crust can cause continental crustal melting. The popular slab break-off model cannot produce volumetrically significant mantle-derived melt and also cannot fix the problem of asthenospheric upwelling without removing the buoyant continental lithospheric mantle to account for the widespread granitic plutons in the Qinling Orogen.

Acknowledgments

We thank Prof. Li Su (the Geologic Lab Center, China University of Geosciences, Beijing) for helping with major and trace elements analysis and zircon LA–ICP–MS U–Pb dating, and Prof. Jinlong Ma (the Guangzhou Institute of Geochemistry, Chinese Academy of Sciences) for the Sr–Nd–Hf isotopic analysis. We also thank editor Sun-Lin Chung for handing this manuscript and Prof. Michael Roden and three anonymous reviewers for constructive comments and suggestions. This study is supported by the National Natural Science Foundation of China (91014003, 41130314).

Appendix 1

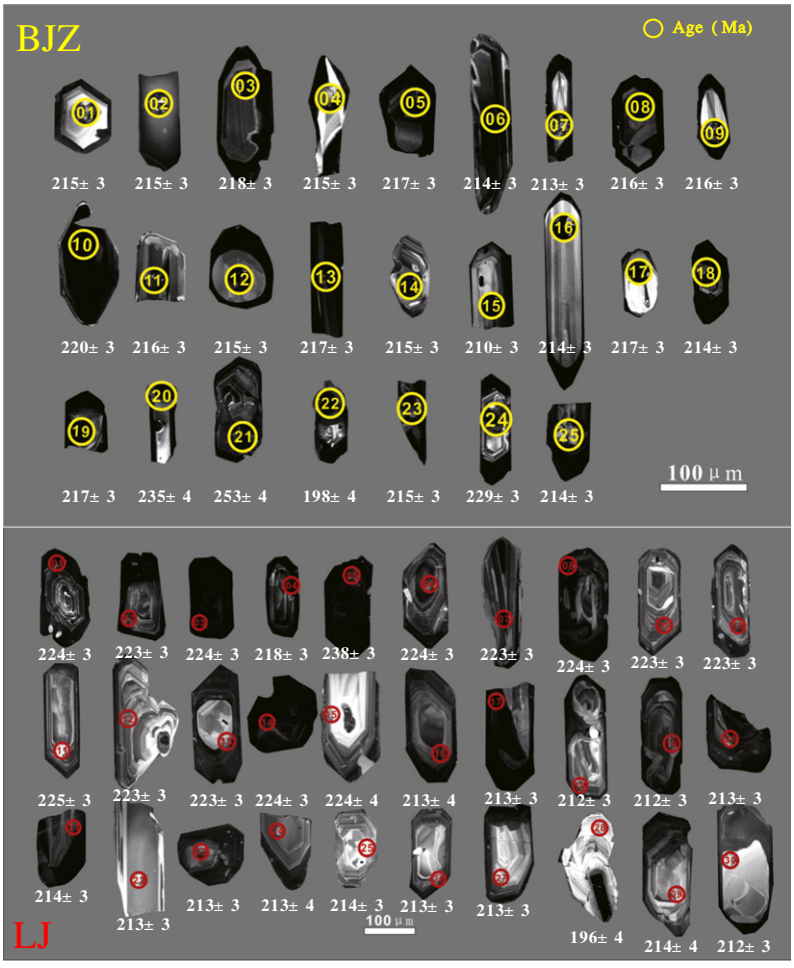

Cathodoluminescence (CL) images of representative zircons from the host granitoids of the BJZ and the LJ plutons. Spots for zircon U–Pb dating using LA–ICP–MS and ages derived from zircons are also shown.

Appendix 2. U–Th–Pb LA-ICP-MS zircon data of granitoids and MME from Baijiazhuang (BJZ) and Lvjing (LJ) pluton

Spot	Content (ppm)				Ratios								Age (Ma)								Discordance
	Th	U	Pb	Th/U	$^{207}Pb/^{206}Pb$	1σ	$^{207}Pb/^{235}U$	1σ	$^{206}Pb/^{238}U$	1σ	$^{208}Pb/^{232}Th$	1σ	$^{207}Pb/^{206}Pb$	1σ	$^{207}Pb/^{235}U$	1σ	$^{206}Pb/^{238}U$	1σ	$^{208}Pb/^{232}Th$	1σ	
BJ4-01	404.9	1441	50.90	0.281	0.0519	0.0012	0.2434	0.0060	0.0340	0.0005	0.0099	0.0003	282	30	221	5	215	3	200	5	2.79%
BJ4-02	140.6	786.9	27.05	0.179	0.0505	0.0014	0.2367	0.0068	0.0340	0.0005	0.0100	0.0004	219	39	216	6	215	3	200	8	0.47%
BJ4-03	92.99	943.8	32.16	0.099	0.0509	0.0013	0.2411	0.0065	0.0344	0.0005	0.0102	0.0005	237	36	219	5	218	3	205	9	0.46%
BJ4-04	254.2	410.5	15.73	0.619	0.0503	0.0020	0.2351	0.0093	0.0339	0.0006	0.0105	0.0003	207	61	214	8	215	3	212	6	−0.47%
BJ4-05	205.0	1084	37.86	0.189	0.0525	0.0013	0.2482	0.0063	0.0343	0.0005	0.0110	0.0003	307	32	225	5	217	3	220	6	3.69%
BJ4-06	399.9	1473	51.40	0.272	0.0520	0.0012	0.2423	0.0058	0.0338	0.0005	0.0099	0.0002	285	29	220	5	214	3	199	5	2.80%
BJ4-07	640.5	982.2	39.53	0.652	0.0721	0.0017	0.3393	0.0084	0.0341	0.0005	0.0121	0.0003	584	122	247	11	213	3	209	3	15.96%
BJ4-08	196.5	806.7	28.31	0.244	0.0509	0.0014	0.2387	0.0066	0.0340	0.0005	0.0112	0.0003	234	37	217	5	216	3	225	6	0.46%
BJ4-09	263.8	720.3	26.09	0.366	0.0536	0.0015	0.2520	0.0072	0.0341	0.0005	0.0106	0.0003	353	37	228	6	216	3	214	6	5.56%
BJ4-10	118.6	2582	87.20	0.046	0.0517	0.0012	0.2468	0.0058	0.0346	0.0005	0.0108	0.0004	271	28	224	5	220	3	216	8	1.82%
BJ4-11	281.7	1069	38.20	0.264	0.0516	0.0013	0.2423	0.0064	0.0340	0.0005	0.0134	0.0003	269	35	220	5	216	3	268	6	1.85%
BJ4-12	267.8	373.5	14.61	0.717	0.0508	0.0019	0.2377	0.0091	0.0340	0.0006	0.0107	0.0003	229	59	217	7	215	3	215	6	0.93%
BJ4-13	572.2	1316	48.59	0.435	0.0535	0.0013	0.2520	0.0063	0.0342	0.0005	0.0109	0.0003	349	31	228	5	217	3	219	5	5.07%
BJ4-14	311.0	1430	49.22	0.218	0.0504	0.0013	0.2353	0.0064	0.0339	0.0005	0.0103	0.0003	211	36	215	5	215	3	207	6	0.00%
BJ4-15	371.1	416.5	16.99	0.891	0.0580	0.0021	0.2673	0.0098	0.0334	0.0005	0.0113	0.0003	176	170	207	14	210	3	210	3	−1.43%
BJ4-16	220.2	500.5	18.17	0.440	0.0504	0.0017	0.2350	0.0082	0.0338	0.0005	0.0105	0.0003	214	51	214	7	214	3	211	6	0.00%
BJ4-17	282.7	477.1	18.25	0.593	0.0535	0.0018	0.2532	0.0085	0.0343	0.0005	0.0106	0.0003	351	48	229	7	217	3	213	6	5.53%
BJ4-18	688.9	3137	116.3	0.220	0.0829	0.0019	0.3939	0.0093	0.0344	0.0005	0.0163	0.0004	889	79	282	8	214	3	207	3	31.78%
BJ4-19	547.4	2135	75.26	0.256	0.0547	0.0012	0.2579	0.0061	0.0342	0.0005	0.0109	0.0003	398	28	233	5	217	3	220	5	7.37%
BJ4-20	863.2	2599	112.7	0.332	0.0966	0.0026	0.5100	0.0140	0.0383	0.0006	0.0181	0.0005	1061	100	329	13	235	4	225	4	40.00%
BJ4-21	905.0	2658	129.4	0.341	0.0995	0.0025	0.5756	0.0146	0.0419	0.0007	0.0233	0.0006	808	118	316	14	253	4	246	4	24.90%
BJ4-22	1436	1342	81.28	1.069	0.2040	0.0048	1.0534	0.0256	0.0374	0.0006	0.0215	0.0005	1112	270	289	32	198	4	188	3	45.96%
BJ4-23	269.3	2206	74.47	0.122	0.0535	0.0012	0.2508	0.0061	0.0340	0.0005	0.0115	0.0003	303	72	223	5	215	3	214	3	3.72%
BJ4-24	197.7	3729	138.9	0.053	0.0682	0.0016	0.3462	0.0085	0.0368	0.0006	0.0340	0.0009	448	78	250	7	229	3	227	6	9.17%
BJ4-25	638.2	1526	68.45	0.418	0.1179	0.0027	0.5895	0.0143	0.0362	0.0005	0.0226	0.0005	773	146	268	15	214	3	208	4	25.23%
DH1-01	432.8	960.2	36.04	0.451	0.0529	0.0011	0.2580	0.0056	0.0354	0.0005	0.0097	0.0002	324	25	233	4	224	3	195	4	4.02%
DH1-02	429.7	1200	44.73	0.358	0.0535	0.0010	0.2597	0.0053	0.0352	0.0005	0.0116	0.0002	260	85	226	7	223	3	222	3	1.35%
DH1-03	164.1	367.8	14.07	0.446	0.0521	0.0014	0.2545	0.0070	0.0354	0.0005	0.0116	0.0003	288	36	230	6	224	3	233	5	2.68%
DH1-04	336.0	939.2	34.12	0.358	0.0520	0.0011	0.2460	0.0055	0.0343	0.0005	0.0115	0.0002	285	26	223	5	218	3	231	5	2.29%
DH1-05	432.6	1412	56.72	0.306	0.0609	0.0011	0.3185	0.0061	0.0379	0.0005	0.0137	0.0003	405	78	254	7	238	3	236	3	6.72%
DH1-06	219.1	367.1	14.58	0.597	0.0521	0.0016	0.2540	0.0081	0.0354	0.0005	0.0118	0.0003	290	45	230	7	224	3	237	5	2.68%
DH1-07	267.7	395.2	15.85	0.677	0.0515	0.0015	0.2498	0.0076	0.0352	0.0005	0.0114	0.0002	265	43	226	6	223	3	230	5	1.35%
DH1-08	431.2	1405	51.96	0.307	0.0555	0.0010	0.2702	0.0055	0.0353	0.0005	0.0114	0.0002	430	22	243	4	224	3	230	4	8.48%
DH1-09	253.3	514.2	19.83	0.493	0.0545	0.0015	0.2643	0.0073	0.0352	0.0005	0.0115	0.0003	390	35	238	6	223	3	232	5	6.73%
DH1-10	210.8	470.3	17.94	0.448	0.0512	0.0015	0.2483	0.0074	0.0352	0.0005	0.0118	0.0003	249	41	225	6	223	3	237	5	0.90%
DH1-11	343.3	453.3	18.88	0.757	0.0552	0.0015	0.2700	0.0075	0.0355	0.0005	0.0119	0.0002	421	35	243	6	225	3	240	5	8.00%
DH1-12	203.4	340.1	13.41	0.598	0.0506	0.0016	0.2455	0.0078	0.0352	0.0006	0.0113	0.0003	221	45	223	6	223	3	228	5	0.00%
DH1-13	199.1	603.4	22.40	0.330	0.0506	0.0013	0.2461	0.0064	0.0353	0.0005	0.0119	0.0003	223	33	223	5	223	3	238	5	0.00%
DH1-14	162.2	424.1	16.00	0.382	0.0510	0.0016	0.2490	0.0079	0.0354	0.0005	0.0115	0.0003	239	45	226	6	224	3	232	6	0.89%
DH1-15	117.3	267.7	10.17	0.438	0.0505	0.0024	0.2458	0.0116	0.0353	0.0006	0.0112	0.0004	218	77	223	9	224	4	226	8	−0.45%
DH1-16	123.0	235.1	8.834	0.523	0.0525	0.0026	0.2434	0.0120	0.0336	0.0006	0.0093	0.0003	309	80	221	10	213	4	187	6	3.76%
DH1-17	397.0	657.3	25.29	0.604	0.0520	0.0015	0.2411	0.0072	0.0336	0.0005	0.0095	0.0002	287	40	219	6	213	3	192	5	2.82%
DH1-18	215.8	571.4	20.62	0.378	0.0507	0.0015	0.2343	0.0071	0.0335	0.0005	0.0093	0.0003	229	41	214	6	212	3	187	5	0.94%
DH1-19	192.7	343.3	12.98	0.561	0.0505	0.0018	0.2328	0.0083	0.0335	0.0006	0.0093	0.0003	216	52	213	7	212	3	188	5	0.47%
DH1-20	179.0	488.9	17.73	0.366	0.0505	0.0015	0.2338	0.0069	0.0336	0.0005	0.0098	0.0003	217	39	213	6	213	3	197	5	0.00%
DH1-21	140.4	372.2	13.58	0.377	0.0506	0.0017	0.2352	0.0080	0.0337	0.0006	0.0098	0.0003	224	49	214	7	214	3	196	6	0.00%
DH1-22	125.3	239.2	9.061	0.524	0.0501	0.0020	0.2319	0.0092	0.0336	0.0006	0.0099	0.0003	201	62	212	8	213	3	200	6	−0.47%
DH1-23	296.4	329.3	13.52	0.900	0.0501	0.0016	0.2322	0.0074	0.0336	0.0005	0.0091	0.0002	198	45	212	6	213	3	184	5	−0.47%
DH1-24	191.7	201.4	8.420	0.952	0.0503	0.0020	0.2335	0.0093	0.0337	0.0006	0.0094	0.0003	209	61	213	8	213	4	189	5	0.00%
DH1-25	144.7	365.8	13.38	0.396	0.0522	0.0016	0.2426	0.0075	0.0337	0.0005	0.0093	0.0003	295	43	221	6	214	3	188	5	3.27%
DH1-26	128.4	519.3	18.21	0.247	0.0507	0.0014	0.2344	0.0066	0.0336	0.0005	0.0096	0.0003	225	37	214	5	213	3	193	6	0.47%
DH1-27	108.4	221.0	8.239	0.491	0.0504	0.0019	0.2333	0.0089	0.0336	0.0006	0.0092	0.0003	212	57	213	7	213	3	185	6	0.00%
DH1-28	80.50	167.4	7.904	0.481	0.1355	0.0045	0.6357	0.0207	0.0340	0.0006	0.0233	0.0007	692	234	239	22	196	4	190	4	21.94%
DH1-29	80.62	143.0	5.382	0.564	0.0506	0.0030	0.2353	0.0137	0.0337	0.0007	0.0084	0.0004	221	98	215	11	214	4	168	8	0.47%
DH1-30	285.5	422.7	16.94	0.675	0.0615	0.0021	0.2841	0.0098	0.0335	0.0006	0.0103	0.0003	657	46	254	8	212	3	207	6	19.81%

Appendix 3. Major elements (wt.%) and trace elements (ppm) compositions of granitoids samples from Baijiazhuang and Lvjing pluton

Pluton	Lvjing								Baijiazhuang						
Rock type	Granitoids						MME		Granitoids						
Sample	DHG12-03	DHG12-10	DHG12-17	DHG12-18	DHG12-20	DHG12-24	DHG12-06	DHG12-09	BJZ12-03	BJZ12-04	BJZ12-05	LZG12-02	LZG12-03	LZG12-05	LZG12-07
SiO_2	70.17	70.07	71.24	69.52	71.95	69.94	62.31	57.07	74.58	76.60	73.47	74.37	72.58	72.86	74.44
TiO_2	0.37	0.34	0.33	0.37	0.25	0.36	0.83	1.10	0.17	0.12	0.17	0.12	0.18	0.15	0.17
Al_2O_3	14.80	14.59	14.45	14.99	14.35	14.76	15.00	16.14	13.15	12.07	13.96	14.04	14.91	14.41	13.63
TFe_2O_3	2.73	2.41	2.52	2.82	1.96	2.57	6.37	6.71	1.30	0.88	1.19	1.06	1.19	1.28	1.08
MnO	0.06	0.05	0.06	0.06	0.05	0.06	0.13	0.18	0.05	0.05	0.05	0.02	0.03	0.05	0.05
MgO	0.91	0.82	0.77	0.91	0.64	0.77	3.32	3.40	0.22	0.16	0.20	0.23	0.27	0.33	0.22
CaO	1.64	1.76	1.84	1.99	1.43	1.90	5.34	5.24	0.98	0.87	0.93	0.82	0.81	0.91	0.62
Na_2O	3.08	3.48	3.27	3.14	3.40	3.43	3.54	3.71	3.63	3.75	3.46	3.07	3.12	3.56	3.42
K_2O	4.74	5.01	4.57	4.41	4.62	5.32	1.42	3.99	5.38	4.89	5.30	5.28	5.17	4.85	5.39
P_2O_5	0.22	0.12	0.13	0.18	0.10	0.15	0.17	0.49	0.07	0.07	0.08	0.14	0.16	0.10	0.12
LOI	0.93	0.62	0.65	0.74	0.63	0.6	0.98	1.17	0.47	0.61	0.59	0.78	0.94	0.79	0.87
Total	99.64	99.28	99.83	99.13	99.38	99.83	99.42	99.20	100.00	100.07	99.40	99.95	99.36	99.29	100.02
Li	68.52	75.76	100.6	52.80	230.2	71.50	29.10	103.4	121.1	130.5	119.7	104.1	71.80	106.7	70.68
Sc	5.456	4.904	5.268	5.566	8.208	5.004	33.68	15.34	1.729	1.871	0.878	2.135	2.56	1.846	1.174
V	39.84	36.46	33.66	38.98	44.04	38.06	203.8	161.4	12.28	4.400	3.700	3.856	5.522	7.874	3.868
Cr	15.66	13.33	11.92	14.84	16.00	13.04	37.88	16.47	3.070	2.652	2.942	6.086	3.156	11.02	2.632
Co	4.586	4.350	3.918	4.802	5.204	4.650	24.40	19.63	1.014	0.459	0.402	0.471	0.578	0.968	0.548
Ni	6.384	4.742	3.892	5.794	6.106	5.372	20.58	10.20	0.941	0.923	2.008	1.889	1.364	7.716	0.794
Cu	2.778	2.448	3.174	2.976	5.940	2.400	8.560	131.2	2.714	1.086	0.966	2.010	2.336	3.856	1.040
Zn	60.20	60.90	63.18	55.22	97.08	42.92	91.84	91.28	71.68	61.94	84.06	57.66	61.90	57.80	76.64
Ga	20.92	21.02	22.48	21.04	45.02	19.24	29.18	20.18	22.60	23.30	20.52	20.69	22.90	22.66	23.46
Rb	290.2	278.0	283.0	254.6	575.4	231.6	96.70	279.4	425.8	424.6	460.6	349.3	363.0	368.4	457.4
Sr	298.4	289.2	257.8	304.6	431.2	289.8	579.8	341.6	105.6	55.98	56.00	58.47	77.44	114.3	61.98
Y	21.68	18.09	18.73	20.26	33.18	15.49	23.24	21.72	25.14	15.53	16.86	13.18	11.49	11.70	11.84
Zr	256.0	210.6	194.4	257.6	350.2	219.2	203.2	281.6	144.3	78.86	105.84	77.31	114.8	124.5	110.6
Nb	22.67	20.59	24.38	21.84	49.60	16.31	14.34	21.02	24.40	22.45	25.20	17.30	21.18	21.84	21.90
Cs	11.56	12.88	24.90	12.35	31.68	9.098	5.930	14.14	17.18	24.96	22.38	21.51	13.07	16.90	9.828
Ba	684.2	635.6	593.4	647.2	1130	638.6	599.2	611.2	458.6	176.3	196.5	240.4	320.8	453.0	271.0
La	36.54	43.50	47.86	49.34	87.40	36.90	26.00	58.82	36.36	27.80	32.26	21.07	34.82	42.30	34.62
Ce	82.96	83.14	88.62	98.66	174.8	88.72	59.76	100.9	70.24	56.52	66.50	43.42	75.34	77.30	70.62
Pr	8.242	9.132	10.32	10.54	17.57	8.090	7.394	12.06	7.284	6.038	7.088	4.732	7.368	7.538	7.678
Nd	30.90	32.66	36.90	37.82	61.80	29.08	30.32	45.10	24.72	20.58	24.38	16.24	25.18	24.46	26.66
Sm	6.438	6.002	6.792	6.954	11.87	5.470	6.448	7.792	4.592	3.928	4.508	3.690	4.980	4.102	5.174
Eu	1.163	1.118	1.073	1.191	1.688	1.112	1.315	1.868	0.495	0.317	0.313	0.350	0.446	0.527	0.420
Gd	5.336	4.812	5.330	5.498	9.512	4.388	5.908	6.510	3.936	3.080	3.510	3.143	3.778	3.138	3.746
Tb	0.711	0.610	0.664	0.692	1.217	0.560	0.803	0.804	0.610	0.452	0.494	0.459	0.464	0.404	0.449
Dy	3.858	3.186	3.370	3.650	6.202	2.922	4.522	4.262	3.800	2.622	2.816	2.388	2.230	2.108	2.164
Ho	0.719	0.597	0.608	0.672	1.091	0.541	0.862	0.792	0.803	0.500	0.543	0.416	0.378	0.375	0.374
Er	2.078	1.731	1.708	1.929	3.034	1.572	2.414	2.236	2.546	1.494	1.602	1.149	1.030	1.068	1.059
Tm	0.297	0.244	0.239	0.274	0.418	0.220	0.314	0.294	0.370	0.215	0.234	0.155	0.138	0.149	0.149
Yb	1.980	1.653	1.595	1.798	2.742	1.435	2.024	1.910	2.332	1.386	1.510	0.972	0.902	0.987	1.012
Lu	0.294	0.246	0.238	0.268	0.400	0.214	0.299	0.284	0.337	0.190	0.210	0.133	0.129	0.143	0.142
Hf	6.159	5.115	4.957	6.134	8.947	5.525	4.940	6.288	3.444	2.142	2.692	2.183	3.026	2.972	2.816
Ta	1.483	1.201	1.524	1.404	3.776	0.991	0.873	1.297	1.612	1.467	1.522	1.130	1.466	1.355	1.486
Pb	31.02	31.64	34.12	29.32	74.46	26.62	10.41	31.08	27.76	29.52	31.34	36.31	32.34	25.92	31.48
Th	26.02	25.48	27.88	28.58	57.76	24.14	5.596	10.84	23.58	17.54	20.26	17.75	27.48	33.54	20.32
U	2.822	6.158	2.692	6.836	7.122	4.292	1.727	4.200	3.588	3.342	7.516	3.575	4.588	3.408	6.468

Appendix 4. Whole-rock Sr–Nd–Hf isotopic composition for granitoids and MME from Baijiazhuang and Lvjing pluton

Pluton	Rock type	Sample	Rb(ppm)	Sr(ppm)	$^{87}Rb/^{86}Sr$	$^{87}Sr/^{86}Sr$	$(^{87}Sr/^{86}Sr)_i$	Sm(ppm)	Nd(ppm)	$^{147}Sm/^{144}Nd$	$^{143}Nd/^{144}Nd$	2 σ	$(^{143}Nd/^{144}Nd)_i$
LJ	MME	DHG12-06	96.7	579.8	0.483	0.71763	0.7161	6.448	30.32	0.129	0.512361	0.000008	0.5122
		DHG12-09	279.4	341.6	2.367	0.71424	0.7068	7.792	45.1	0.105	0.512255	0.000007	0.5121
	Granitoids	DHG12-10	278	289.2	2.782	0.71567	0.7070	6.002	32.66	0.112	0.512279	0.000009	0.5121
		DHG12-18	254.6	304.6	2.419	0.71484	0.7073	6.954	37.82	0.112	0.512269	0.000011	0.5121
		DHG12-20	575.4	431.2	3.862	0.72	0.7079	11.87	61.8	0.117	0.512249	0.000007	0.5121
		DHG12-24	231.6	289.8	2.313	0.71447	0.7072	5.47	29.08	0.114	0.512286	0.000011	0.5121
BJZ	Granitoids	BJZ12-03	425.8	105.6	11.67	0.74156	0.7050	4.592	24.72	0.113	0.512082	0.000010	0.5119
		BJZ12-04	424.6	55.98	21.95	0.77061	0.7019	3.928	20.58	0.116	0.512071	0.000008	0.5119
		LZG12-02	349.3	58.47	17.29	0.76093	0.7068	3.69	16.24	0.138	0.512060	0.000008	0.5119
		LZG12-05	368.4	114.3	9.328	0.73546	0.7063	4.102	24.46	0.102	0.511954	0.000009	0.5118
		LZG12-07	457.4	61.98	21.36	0.77009	0.7033	5.147	26.66	0.118	0.511963	0.000010	0.5118

$(^{87}Sr/^{86}Sr)_i = (^{87}Sr/^{86}Sr)_{Sample} - {}^{87}Rb/^{86}Sr(e^{\lambda t} - 1)$, $\lambda = 1.42 \times 10^{-11}a^{-1}$, $t = 220$ Ma.
$(^{143}Nd/^{144}Nd)_i = (^{143}Nd/^{144}Nd) - (^{147}Sm/^{144}Nd) \times (e^{\lambda t} - 1)$, $\varepsilon_{Nd}(t) = [(^{143}Nd/^{144}Nd) / (^{143}Nd/^{144}Nd)_{CHUR}(t) - 1] \times 10^4$, $(^{143}Nd/^{144}Nd)_{CHUR}(t) = 0.512638–0.1967 \times (e^{\lambda t} - 1)$, $T_{DM} = 1/\lambda \times \ln\{1 + [((^{143}Nd/^{144}Nd) - 0.51315) / ((^{147}Sm/^{144}Nd) - 0.21317)]\}$, $\lambda_{Sm\text{-}Nd} = 6.54 \times 10^{-12}a^{-1}$.
$(^{176}Hf/^{177}Hf)_i = [(^{176}Hf/^{177}Hf) - (^{176}Lu/^{177}Hf) \times (e^{\lambda t} - 1)$, $\varepsilon_{Hf}(t) = [(^{176}Hf/^{177}Hf) / (^{176}Hf/^{177}Hf)_{CHUR}(t) - 1] \times 10^4$, $T_{DM1} = 1/\lambda \times \ln[1 + ((^{176}Hf/^{177}Hf)_{Sample} - (^{176}Hf/^{177}Hf)_{DM})/((^{176}Lu/^{177}Hf)_{Sample} - (^{176}Lu/^{177}Hf)_{DM})]$, $T_{DM2} = T_{DM1} - (T_{DM1} - t)((f_{CC} - f_{Sample}) / (f_{CC} - f_{DM}))$, $f_{Lu\text{-}Hf} = (^{176}Lu/^{177}Hf)_{Sample} / (^{176}Lu/^{177}Hf)_{CHUR}$-1, $(^{176}Lu/^{177}Hf)_{CHUR} = 0.0332$, $(^{176}Hf/^{177}Hf)_{CHUR, 0} = 0.282785$, $(^{176}Lu/^{177}Hf)_{DM} = 0.0384$, $(^{176}Hf/^{177}Hf)_{DM} = 0.28325$, f_{CC}, f_{Sample}, f_{DM} are their own $f_{Lu\text{-}Hf}$, $\lambda = 1.867 \times 10^{-11}a^{-1}$.

Appendix 4 (*continued*)

Pluton	Rock type	$\varepsilon_{Nd}(t)$	T_{DM}(Ma)	Lu(ppm)	Hf(ppm)	$^{176}Lu/^{177}Hf$	$^{176}Hf/^{177}Hf$	2 σ	$(^{176}Hf/^{177}Hf)_i$	$\varepsilon_{Hf}(t)$	T_{DM1} (Ma)	T_{DM2} (Ma)
LJ	MME	−3.52	1425	0.299	4.94	0.009	0.282739	0.000005	0.2827	2.41	911	1160
		−4.90	1256	0.284	6.288	0.006	0.282624	0.000006	0.2826	−1.34	1039	1419
	Granitoids	−4.62	1302	0.246	5.115	0.007	0.282602	0.000004	0.2826	−2.18	1089	1468
		−4.82	1318	0.268	6.134	0.006	0.282607	0.000005	0.2826	−1.91	1060	1457
		−5.35	1417	0.4	8.947	0.006	0.282560	0.000006	0.2825	−3.59	1142	1563
		−4.56	1326	0.214	5.525	0.005	0.282609	0.000005	0.2826	−1.74	1034	1453
BJZ	Granitoids	−8.50	1614	0.337	3.444	0.014	0.282457	0.000005	0.2824	−8.33	1705	1788
		−8.80	1682	0.19	2.142	0.013	0.282485	0.000004	0.2824	−7.15	1565	1727
		−9.64	2194	0.133	2.183	0.009	0.282492	0.000003	0.2825	−6.33	1348	1714
		−10.69	1629	0.143	2.972	0.007	0.282377	0.000005	0.2823	−10.14	1462	1971
		−10.95	1875	0.142	2.816	0.007	0.282429	0.000004	0.2824	−8.35	1390	1855

References

Barbarin, B., 1999. A review of the relationships between granitoid types, their origins and their geodynamic environments. Lithos 46, 605–626.

Barbarin, B., 2005. Mafic magmatic enclaves and mafic rocks associated with some granitoids of the central Sierra Nevada batholith, California: nature, origin, and relations with the hosts. Lithos 80, 155–177.

Baxter, S., Feely, M., 2002. Magma mixing and mingling textures in granitoids: examples from the Galway Granite, Connemara, Ireland. Mineralogy and Petrology 76, 63–74.

Bird, P., 1979. Continental delamination and the Colorado Plateau. Journal of Geophysical Research 84, 7561–7571.

Cao, X., Lü, X., Yao, S., Mei, W., Zou, X., Chen, C., Liu, S., Zhang, P., Su, Y., Zhang, B., 2011. LA–ICP–MS U–Pb zircon geochronology, geochemistry and kinetics of the Wenquan ore-bearing granites from West Qinling, China. Ore Geology Reviews 43, 120–131.

Chen, S., Niu, Y., Sun, W., Zhang, Y., Li, J., Guo, P., Sun, P., 2015. On the origin of mafic magmatic enclaves (MMEs) in syn-collisional granitoids: evidence from the Baojishan pluton in the North Qilian Orogen, China. Mineralogy and Petrology 1–20.

Corfu, F., Hanchar, J., Hoskin, P., Kinny, P., 2003. Atlas of zircon textures. Reviews in Mineralogy and Geochemistry 53, 469–500.

Davidson, J.P., 1996. Deciphering mantle and crustal signatures in subduction zone magmatism. Subduction top to bottom, pp. 251–262.

Davies, J., von Blanckenburg, F., 1995. Slab breakoff: a model of lithosphere detachment and its test in the magmatism and deformation of collisional orogens. Earth and Planetary Science Letters 129, 85–102.

Dong, Y., Zhang, G., Neubauer, F., Liu, X., Genser, J., Hauzenberger, C., 2011. Tectonic evolution of the Qinling orogen, China: review and synthesis. Journal of Asian Earth Sciences 41, 213–237.

Dong, Y., Liu, X., Santosh, M., Chen, Q., Zhang, X., Li, W., He, D., Zhang, G., 2012a. Neoproterozoic accretionary tectonics along the northwestern margin of the Yangtze Block, China: constraints from zircon U–Pb geochronology and geochemistry. Precambrian Research 196, 247–274.

Dong, Y., Liu, X., Neubauer, F., Zhang, G., Ni, T., Zhang, Y., Zhang, X., Li, W., 2013. Timing of Paleozoic amalgamation between the North China and South China Blocks: evidence from detrital zircon U–Pb ages. Tectonophysics 586, 173–191.

Elliott, T., 2003. Tracers of the slab. Inside the subduction factory, pp. 23–45.

Ernst, W., Liou, J., 1995. Contrasting plate-tectonic styles of the Qinling–Dabie–Sulu and Franciscan metamorphic belts. Geology 23, 353–356.

Ernst, W., Tsujimori, T., Zhang, R., Liou, J., 2007. Permo-Triassic collision, subduction-zone metamorphism, and tectonic exhumation along the East Asian continental margin. Annual Review of Earth and Planetary Sciences 35, 73–110.

Faure, M., Lin, W., Monié, P., Meffre, S., 2008. Palaeozoic collision between the North and South China blocks, Triassic intracontinental tectonics, and the problem of the ultrahigh-pressure metamorphism. Comptes Rendus Geoscience 340, 139–150.

Geological Map 1/250,000 (2007) (Chinese Geological Regional Survey and Geological Investigation Institute of Gansu Province).

Harris, N., Pearce, J., Tindle, A., 1986. Geochemical characteristics of collision-zone magmatism. Geological Society, London, Special Publications 19, 67–81.

Huang, H., Niu, Y., Nowell, G., Zhao, Z., Yu, X., Zhu, D., Mo, X., Ding, S., 2014. Geochemical constraints on the petrogenesis of granitoids in the East Kunlun Orogenic belt, northern Tibetan Plateau: implications for continental crust growth through syn-collisional felsic magmatism. Chemical Geology 370, 1–18.

Jiang, C., 1994. On Major Tectonic Characteristics of the Central Orogenic Belt. Dixue Yanjiu 2 (in Chinese).

Jiang, Y., Jin, G., Liao, S., Zhou, Q., Zhao, P., 2010. Geochemical and Sr–Nd–Hf isotopic constraints on the origin of Late Triassic granitoids from the Qinling orogen, central China: implications for a continental arc to continent-continent collision. Lithos 117, 183–197.

Johnson, M.C., Plank, T., 2000. Dehydration and melting experiments constrain the fate of subducted sediments. Geochemistry, Geophysics, Geosystems 1, 1–26.

Klein, E., Langmuir, C., 1987. Global correlations of ocean ridge basalt chemistry with axial depth and crustal thickness. Journal of Geophysical Research 92, 8089–8115.

Lai, S., Qin, J., Chen, L., Grapes, R., 2008. Geochemistry of ophiolites from the Mian-Lue Suture Zone: implications for the tectonic evolution of the Qinling Orogen, Central China. International Geology Review 50, 650–664.

Lee, C.-T., Anderson, D., 2015. Continental crust formation at arcs, the arclogite "delamination" cycle, and one origin for the fertile melting anomalies in the mantle. Science Bulletin 60 (13), 1141–1156.

Li, X., Li, Z., Li, W., Wang, Y., 2006. Initiation of the Indosinian Orogeny in South China: evidence for a Permian magmatic arc on Hainan Island. The Journal of Geology 114, 341–353.

Li, S., Sun, W., 1996. A Middle Silurian-Early Devonian magmatic arc in the Qinling Mountains of central China: A discussion. The Journal of geology 501–503.

Li, S., Kusky, T., Wang, L., Zhang, G., Lai, S., Liu, X., Dong, S., Zhao, G., 2007. Collision leading to multiple-stage large-scale extrusion in the Qinling orogen: insights from the Mianlue suture. Gondwana Research 12, 121–143.

Li, X., Li, W., Li, Z., Lo, C., Wang, J., Ye, M., Yang, Y., 2009. Amalgamation between the Yangtze and Cathaysia Blocks in South China: constraints from SHRIMP U–Pb zircon ages, geochemistry and Nd–Hf isotopes of the Shuangxiwu volcanic rocks. Precambrian Research 174, 117–128.

Ludwig, K., 2003. User's manual for Isoplot 3.00: a geochronological toolkit for Microsoft Excel. Kenneth R. Ludwig.

Maniar, P., Piccoli, P., 1989. Tectonic discrimination of granitoids. Geological Society of America Bulletin 101, 635–643.

Mattauer, M., Matte, P., Malavieille, J., Tapponnier, P., Maluski, H., Qin, X., Lun, L., Qin, T., 1985. Tectonics of the Qinling belt: build-up and evolution of eastern Asia. Nature 317, 496–500.

McKenzie, D., Bickle, D., 1988. The volume and composition of melt generated by extension of the lithosphere. Journal of Petrology 29 (3), 625–679.

Meng, Q., Zhang, G., 1999. Timing of collision of the North and South China blocks: controversy and reconciliation. Geology 27, 123–126.

Meng, Q., Zhang, G., 2000. Geologic framework and tectonic evolution of the Qinling orogen, central China. Tectonophysics 323, 183–196.

Morris, J., Leeman, W., Tera, F., 1990. The subducted component in island arc lavas: constraints from Be isotopes and B-Be systematics. Nature 344, 31–36.

Nichols, G.T., Wyllie, P.J., Stern, C.R., 1994. Subduction zone melting of pelagic sediments constrained by melting experiments. Nature 371, 785–788.

Niu, Y., Batiza, R., 1991. An empirical method for calculating melt compositions produced beneath mid-ocean ridges: Application for axis and off-axis (seamounts) melting. Journal of Geophysical Research 96 (21), 753–777.

Niu, Y., 2005. Generation and evolution of basaltic magmas: some basic concepts and a new view on the origin of Mesozoic–Cenozoic basaltic volcanism in eastern China. Geological Journal of China Universities 11, 9–46.

Niu, Y., O'Hara, M., 2008. Global correlations of ocean ridge basalt chemistry with axial depth: a new perspective. Journal of Petrology 49, 633–664.

Niu, Y., O'Hara, M., 2009. MORB mantle hosts the missing Eu (Sr, Nb, Ta and Ti) in the continental crust: new perspectives on crustal growth, crust–mantle differentiation and chemical structure of oceanic upper mantle. Lithos 112, 1–17.

Niu, Y., O'Hara, M., Pearce, J., 2003. Initiation of subduction zones as a consequence of lateral compositional buoyancy contrast within the lithosphere: a petrological perspective. Journal of Petrology 44, 851–866.

Niu, Y., Zhao, Z., Zhu, D., Mo, X., 2013. Continental collision zones are primary sites for net continental crust growth-A testable hypothesis. Earth-Science Reviews 127, 96–110.

Pearce, J.A., Peate, D.W., 1995. Tectonic implications of the composition of volcanic arc magmas. Annual Review of Earth and Planetary Sciences 23, 251–286.

Pearce, J., Harris, N., Tindle, A., 1984. Trace element discrimination diagrams for the tectonic interpretation of granitic rocks. Journal of Petrology 25, 956–983.

Pupin, J., 1980. Zircon and granite petrology. Contributions to Mineralogy and Petrology 73, 207–220.

Qin, J., Lai, S., Li, Y., 2008a. Post-collisional plutonism with adakitic signatures: the Triassic Yangba granodiorite (Bikou terrane, northern Yangtze Block). Chinese Journal of Geochemistry 27, 72–81.

Qin, J., Lai, S., Li, Y., 2008b. Slab breakoff model for the Triassic post-collisional adakitic granitoids in the Qinling Orogen, Central China: zircon U–Pb ages, geochemistry, and Sr–Nd–Pb isotopic constraints. International Geology Review 50, 1080–1104.

Qin, J., Lai, S., Grapes, R., Diwu, C., Ju, Y., Li, Y., 2009. Geochemical evidence for origin of magma mixing for the Triassic monzonitic granite and its enclaves at Mishuling in the Qinling orogen (central China). Lithos 112, 259–276.

Ratschbacher, L., Hacker, B., Calvert, A., Webb, L., Grimmer, J., McWilliams, M., Ireland, T., Dong, S., Hu, J., 2003. Tectonics of the Qinling (Central China): tectonostratigraphy, geochronology, and deformation history. Tectonophysics 366, 1–53.

Rudnick, R., Gao, S., 2003. Composition of the continental crust. Treatise on Geochemistry 3, 1–64.

Song, S., Niu, Y., Wei, C., Ji, J., Su, L., 2010a. Metamorphism, anatexis, zircon ages and tectonic evolution of the Gongshan block in the northern Indochina continent-an eastern extension of the Lhasa Block. Lithos 120, 327–346.

Song, S., Su, L., Li, X., Zhang, G., Niu, Y., Zhang, L., 2010b. Tracing the 850 Ma continental flood basalts from a piece of subducted continental crust in the North Qaidam UHPM belt, NW China. Precambrian Research 183, 805–816.

Sun, S., McDonough, W., 1989. Chemical and isotopic systematics of oceanic basalts: implications for mantle composition and processes. Geological Society, London, Special Publications 42, 313–345.

Sun, W., Li, S., Zhang, H., Gao, S., Zhang, B., Luo, T., Ling, W., 1998. Pb isotopes of granitoids suggest Devonian accretion of the Yangtze (South China) craton to North China craton: comment and reply. Geology 29, 859–861.

Sun, W., Li, S., Chen, Y., Li, Y., 2002. Timing of synorogenic granitoids in the South Qinling, Central China: constraints on the evolution of the Qinling–Dabie Orogenic Belt. The Journal of geology 110, 457–468.

Vernon, R., 1984. Microgranitoid Enclaves in Granites-Globules of Hybrid Magma Quenched in a Plutonic Environment. Nature 309, 438–439.

Vroon, P., Bergen, M.V., White, W., Varekamp, J., 1993. Sr–Nd–Pb isotope systematics of the Banda Arc, Indonesia: combined subduction and assimilation of continental material. Journal of Geophysical Research: Solid Earth 98 (12), 22349–22366.

Wang, X., Wang, T., Zhang, C., 2013. Neoproterozoic, Paleozoic, and Mesozoic granitoid magmatism in the Qinling Orogen, China: constraints on orogenic process. Journal of Asian Earth Sciences 72, 129–151.

Wiedenbeck, M., Alle, P., Corfu, F., Griffin, W., Meier, M., Oberli, F., Quadt, A., Roddick, J., Spiegel, W., 1995. Three natural zircon standards for U–Th–Pb, Lu–Hf, trace element and REE analyses. Geostandards Newsletter 19, 1–23.

Xiao, Q., Qiu, R., Deng, J., Li, T., Mo, X., Hong, D., Lu, X., Wang, T., Wu, F., Xie, C., 2005. Granitoids and continental crustal growth modes in China. Geology in China 32 (3), 343–352 (in Chinese with English abstract).

Xiao, Q., Deng, J., Qiu, R., Liu, Y., Feng, Y., 2009. A preliminary study of the relationship between granitoids and the growth of continental crust: a case study of the formation of key orogen granitoids in China. Geology in China 36 (3), 594–622 (in Chinese with English abstract).

Xu, J., Castillo, P., Li, X., Yu, X., Zhang, B., Han, Y., 2002. MORB-type rocks from the Paleo-Tethyan Mian–Lueyang northern ophiolite in the Qinling Mountains, central China:

implications for the source of the low $^{206}Pb/^{204}Pb$ and high $^{143}Nd/^{144}Nd$ mantle component in the Indian Ocean. Earth and Planetary Science Letters 198, 323–337.

Xu, Y., Mao, Y., Wang, G., 2006. Discuss on diagenetic and metallogenic features and metallogenic mechanism of Baijiazhaung Rock Mass in Minxian–Lixian area of Gansu Province. Gansu Geology 15 (2), 36–41 (in Chinese with English abstract).

Xue, F., Kröner, A., Reischmann, T., Lerch, F., 1996. Palaeozoic pre-and post-collision calc-alkaline magmatism in the Qinling orogenic belt, central China, as documented by zircon ages on granitoid rocks. Journal of the Geological Society 153, 409–417.

Yang, L., Deng, J., Qiu, K., Ji, X., Santosh, M., Song, K., Song, Y., Geng, J., Zhang, C., Hua, B., 2014. Magma mixing and crust–mantle interaction in the Triassic monzogranites of Bikou Terrane, central China: constraints from petrology, geochemistry, and zircon U–Pb-Hf isotopic systematics. Journal of Asian Earth Sciences 98, 320–341.

Zhang, G., Liu, X, 1998. Some remarks on China Central Orogenic system. Earth Science Froniers (China University of Geosciences, Beijing), 9–14 (in Chinese with English abstract).

Zhang, G., Cheng, S., Guo, A., Dong, Y., Lai, S., Yao, A., 2004a. Mianlue paleo-suture on the southern margin of the Central Orogenic System in Qinling–Dabie with a discussion of the assembly of the main part of the continent of China. Geological Bulletin of China, 846–853 (in Chinese with English abstract).

Zhang, G., Guo, A., Yao, A., 2004b. Western Qinling–Songpan continental tectonic node in China's continental tectonics. Earth Science Froniers (China University of Geosciences, Beijing), 23–32 (in Chinese with English abstract).

Zhang, Z., Zhang, G., Liu, D., Wang, Z., Tang, S., Wang, J., 2006. Isotopic Geochronology and Geochemistry of ophilites, Granites and Clastic Sedimentary Rocks in the Qinling Orogenic Belt. Geological Publishiing Home, pp. 1–348.

Zhang, H., Jin, L., Zhang, L., Nigel, H., Zhou, L., Hu, S., Zhang, B., 2007. Geochemical and Pb–Sr–Nd isotopic compositions of granitoids from western Qinling belt: constraints on basement nature and tectonic affinity. Science in China Series D: Earth Sciences 50, 184–196.

Zhang, R., Liou, J., Ernst, W., 2009. The Dabie–Sulu continental collision zone: a comprehensive review. Gondwana Research 16, 1–26.

Zhu, X., Chen, F., Li, S., Yang, Y., Nie, H., Siebel, W., Zhai, M., 2011. Crustal evolution of the North Qinling terrain of the Qinling Orogen, China: evidence from detrital zircon U–Pb ages and Hf isotopic composition. Gondwana Research 20, 194–204.